JACS
JOURNAL OF THE AMERICAN CHEMICAL SOCIETY
Article
pubs.acs.org/JACS

Improving the Second-Order Nonlinear Optical Response of Fluorescent Proteins: The Symmetry Argument

Evelien De Meulenaere,[†,‡,§] Ngan Nguyen Bich,[⊥] Marc de Wergifosse,[∥] Kristof Van Hecke,[⊥,#] Luc Van Meervelt,[⊥] Jozef Vanderleyden,[†,§] Benoît Champagne,[∥] and Koen Clays*[,‡,§]

[†]Centre of Microbial and Plant Genetics, KU Leuven, Kasteelpark Arenberg 20, BE-3001 Leuven, Belgium

[‡]Laboratory for Molecular Electronics and Photonics, Department of Chemistry, KU Leuven, Celestijnenlaan 200D, BE-3001 Leuven, Belgium

[§]Institute for Nanoscale Physics and Chemistry, KU Leuven, Belgium

[⊥]Biomolecular Architecture, Department of Chemistry, KU Leuven, Celestijnenlaan 200F, BE-3001 Leuven, Belgium

[∥]Laboratoire de Chimie Théorique, University of Namur, Rue de Bruxelles 61, BE-5000 Namur, Belgium

Supporting Information

ABSTRACT: We have successfully designed and expressed a new fluorescent protein with improved second-order nonlinear optical properties. It is the first time that a fluorescent protein has been rationally altered for this particular characteristic. On the basis of the specific noncentrosymmetry requirements for second-order nonlinear optical effects, we had hypothesized that the surprisingly low first hyperpolarizability (β) of the enhanced yellow fluorescent protein (eYFP) could be explained by centrosymmetric stacking of the chromophoric Tyr66 and the neighboring Tyr203 residue. The inversion center was removed by mutating Tyr203 into Phe203, with minor changes in the linear optical properties and even an improved fluorescence quantum yield. Structure determination by X-ray crystallography as well as linear optical characterization corroborate a correct folding and maturation. Measurement of β by means of hyper-Rayleigh scattering (HRS) as well as their analysis using quantum chemistry calculations validate our hypothesis. This observation can eventually lead to improved red fluorescent proteins for even better performance. On the basis of the specific function (second-harmonic generation), the color of its emission, and in analogy with the "fruit" names, we propose SHardonnay as the name for this Tyr203Phe mutant of eYFP.

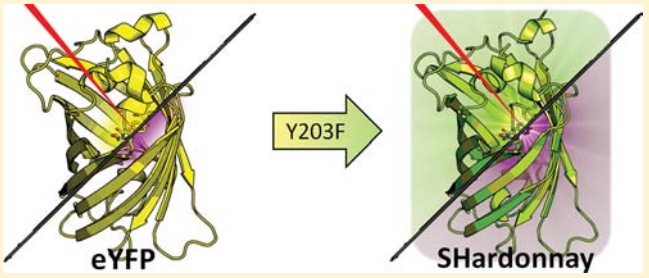

INTRODUCTION

Second-harmonic imaging microscopy (SHIM) is a rapidly emerging imaging technique[1−4] in biomedical research, usually based on contrast created by intrinsic nonlinear optical properties of certain molecules (collagen, myosin, tubulin, and starch). We previously showed that fluorescent proteins exhibit a considerable second-harmonic generation (SHG) response,[5−8] and we are investigating the implementation of fluorescent proteins for SHIM. In our selection, we had observed that enhanced yellow fluorescent protein (eYFP) exhibits poor SHG performance compared to other related fluorescent proteins. We speculated that this could be due to the centrosymmetric arrangement of two π-stacked tyrosine residues in the chromophore.[6] In an effort to improve the second-order nonlinear optical properties of eYFP, we have now replaced the Tyr203 residue by Phe203, giving rise to a new fluorescent protein with a minor blue shift of 2 nm in the absorption and 3 nm in the emission spectrum compared to the parent eYFP.

The advantages of nonlinear imaging techniques based on two-photon excited fluorescence and SHG include low absorption, low scattering and hence higher penetration depth in the sample, lower phototoxicity, reduced out-of-focus photobleaching, and higher intrinsic axial resolution associated with a quadratic intensity profile.[9−11] The additional value of SHIM is the collection of structural information and the opportunity to image highly ordered (labeled and unlabeled) structures in a cellular context.[12−18] SHIM has been previously used to image small conformational changes in singly labeled proteins upon binding to ligands, e.g., with an incorporated non-natural amino acid.[19] Additionally, SHIM is polarization-sensitive[20−23] and allows the determination of the pitch angle of helical molecules, as well as the effective orientation of aligned dipolar chromophores. However, SHIM with live labeled samples is currently limited to the labeling of cellular membranes (but not limited to the plasmamembrane[24]) and the use of voltage-sensitive dyes.[25−28] The power of SHIM lies in the coherent nature of the signal, causing a drastic reaction to small changes in the local centrosymmetry or in the membrane potential. To this purpose, dyes are being designed in an attempt to combine good amphiphylicity, high hyper-

Received: January 7, 2013
Published: February 13, 2013

dx.doi.org/10.1021/ja400098b | J. Am. Chem. Soc. 2013, 135, 4061−4069

polarizabilities, high voltage sensitivity, and low internalization rates, often based on the structure−property relationship in push−pull chromophores.[26,29,30] Because it was shown previously that enhanced green fluorescent protein (eGFP) meets these properties,[31] we directed our attention to fluorescent proteins as possible in vivo markers to visualize membrane potentials. Many variations of fluorescent proteins with different optical properties have been developed in the past for varying purposes[32−38] but not for the second-order nonlinear optical properties. Tuning of the linear spectral properties is usually based on the variation of the length of the effective conjugation path in the chromophore. This is usually achieved by extending the covalent conjugated system but also by more subtle alterations such as varying the bond length alternation of single and double bonds in the chromophore[39] or by noncovalent interaction (e.g., π-stacking in eYFP[40] and Venus[41]).

We have demonstrated earlier that the chromophore embedded in the protein matrix of bacteriorhodopsin is noncentrosymmetric and capable of generating second-harmonic scattering.[42] On the basis of the similarity with fluorescent proteins (a noncentrosymmetric chromophore in a protective protein barrel), we measured the second-order nonlinear optical response for a selection of the rainbow of fluorescent proteins: eGFP, eYFP, DsRed, mStrawberry, mCherry, and the photoswitchable Dronpa.[5−8] We have observed a general trend in the relationship between their linear optical properties and the first hyperpolarizability, β, being a measure for the second-order nonlinear optical properties. Knowing that a red shift of the spectral properties of the chromophore is linked to a more extended conjugated system, we expected this to coincide with an increasing β, and this was demonstrated for all fluorescent proteins except eYFP. The extremely low β of eYFP could possibly be due to the molecular structure of its chromophore, containing an inversion center, turning half the chromophore into a centrosymmetric structure. In an effort to validate this hypothesis and find a yellow fluorescent protein with an appreciable β, we found zFP538, a natural yellow-to-orange fluorescent protein isolated by Matz and coworkers (chromophore displayed in Figure 1e and 1f).[43] Our hypothesis also inspired the generation of an eYFP mutant, eliminating the centrosymmetry in the eYFP chromophore by replacing Tyr203 (Figure 1a and 1b) with Phe203 (Figure 1c and 1d) through site-directed mutagenesis. The mutant was named SHardonnay for its improved second-harmonic properties and for its color appearance similar to white wine of the Chardonnay grape. SHardonnay was thoroughly characterized, both by optical measurements and by X-ray crystallography, and the linear and second-order nonlinear optical properties were corroborated by advanced theoretical methods.

RESULTS

Experimental Linear Optical Characterization. With linear spectroscopy, we determined that the absorption maximum of SHardonnay is at 511 nm, and the emission maximum at 524 nm (Figure 2 and Table 1), a minor hypsochromic shift with respect to eYFP, which is even visible to the eye. This observation already implies that the folding of the protein is not compromised and the chromophore formation is supported by the new microenvironment of the chromophore. The spectral difference between the two yellow FPs and zFP538, respectively, is markedly larger, giving zFP538

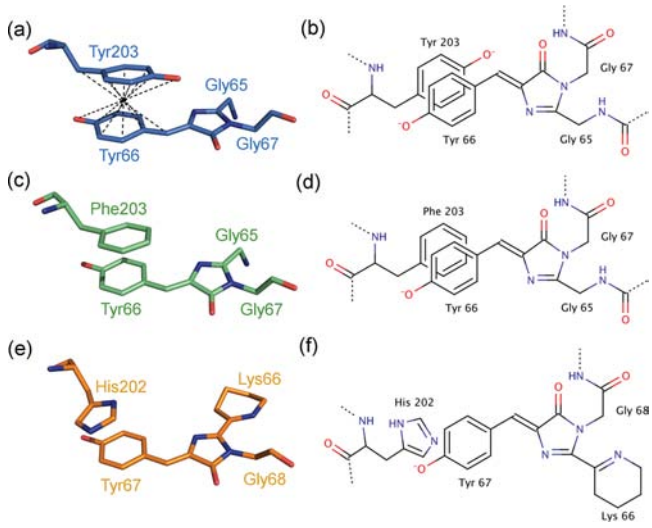

Figure 1. Representation of the different chromophores discussed in the paper. (a) The chromophore of eYFP was taken from PDB ID 1YFP,[40] (c) the structure of SHardonnay was submitted to the protein database as 3V3D, and (e) the chromophore of zFP538 was taken from PDB ID 2OGR.[44] Parts b, d, and f show the respective chemical structures in 2D. The presence of an inversion center in the eYFP chromophore is marked by dashed lines in image a. Images a, c, and e were generated with PyMol.[45]

a clear orange color. We assessed and approved the purity of the samples based on SDS-PAGE (sodium dodecyl sulfate polyacrylamide gel electrophoresis) and mass spectrometry results. With a more extensive characterization of the fluorescent protein in mind, we also determined a number of other important characteristics of SHardonnay (Table 1). We measured a fluorescence lifetime of 3.4 ns, which is typical for GFP-like proteins, an extinction coefficient at the absorption peak of the chromophore (511 nm) of around 89 000 $M^{-1}cm^{-1}$, compared to 83 400 $M^{-1}cm^{-1}$ for eYFP, and a quantum yield of 0.75, remarkably higher than that of eYFP. The small increase in the extinction coefficient could be explained by the absolute absence of a peak around 400 nm (see Figure 2).

X-ray Diffraction. The structure of SHardonnay has been solved to a resolution of 1.95 Å. The overall structure of the mutant shows the 11-stranded β-barrel fold typical for GFP-like proteins, with the chromophore suspended in the center by a coaxial helix. The protein consists of 238 amino acid residues, of which residues 2−231 could be clearly defined in the electron density map, including four additional residues of the C-terminus, in comparison with its parent eYFP (PDB ID 1YFP).[40] These residues are positioned in a hydrophobic cleft of one of the adjacent protomers in the lattice, rendering them more rigid and more easily and unambiguously modeled in the electron density map. The root-mean-square (rms) deviation between the eYFP and the SHardonnay α carbons is 0.28 Å, and no considerable movement of either the backbone or the side chains is detected inside the β-barrel. Superposition of the α carbons of SHardonnay and zFP538 (PDB ID 2OGR),[44] results in an rms deviation of 1.51 Å for 210 equivalent positions, with large differences in solvent exposing loop configurations, which is consistent with the low sequence identity of 22% (PDBeFold)[51] compared to zFP538.[43,52]

Unlike most other fluorescent proteins, whose chromophore consists of a single moiety, arising from a post-translational

dx.doi.org/10.1021/ja400098b | J. Am. Chem. Soc. 2013, 135, 4061−4069

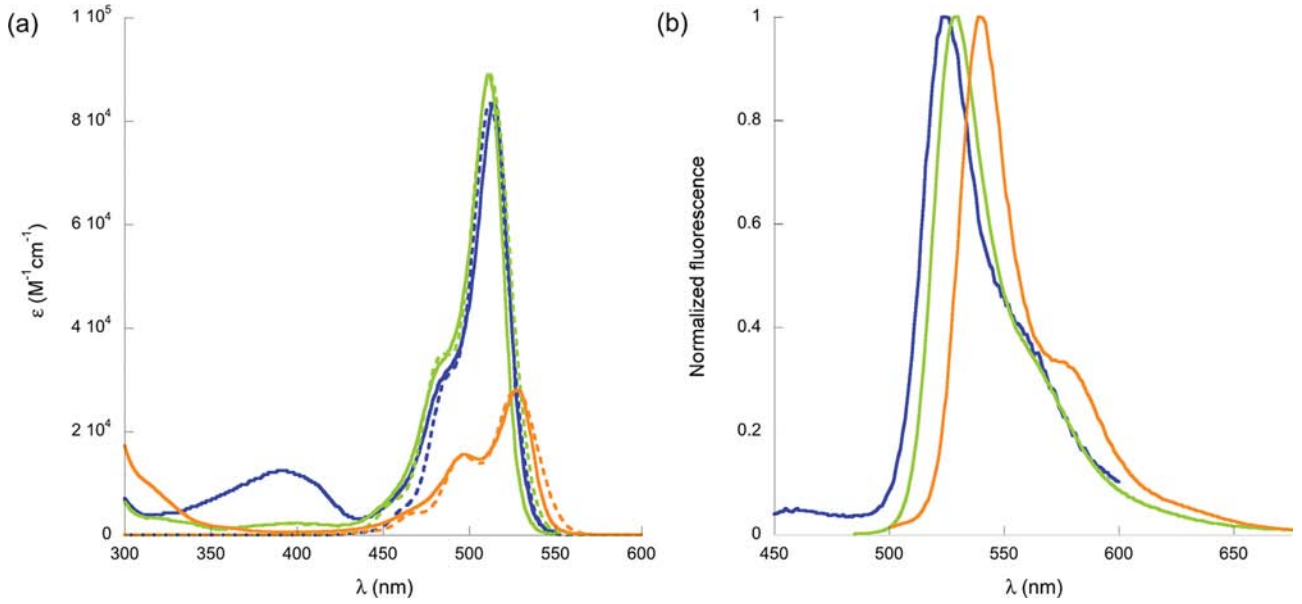

Figure 2. Linear spectral properties of the fluorescent proteins discussed in the paper. (a) Extinction coefficients and (b) normalized fluorescence spectra of the fluorescent proteins eYFP (blue), SHardonnay (green), and zFP538 (orange), all measured under the same conditions. Full lines show experimental data, while the dashed lines represent simulated spectra, scaled for the same maximum value.

Table 1. Experimentally Determined and Calculated Linear and Nonlinear Spectral Characteristics

	eYFP	SHardonnay	zFP538
$\lambda_{abs,max}$ (nm)	514	511	528
$\lambda_{em,max}$ (nm)	527	524	538
ε at $\lambda_{abs,max}$ (M^{-1} cm^{-1})	83 400	89 000	20 200[43]
τ (ns)	2.9−3.4[a]	3.4[b]	ND
Φ	0.60[33]	0.75	0.42[43]
PDB ID	1YFP[40]	3V3D	2OGR[44]
θ (deg)	14.5	18.1	19.4
γ (deg)	12.1	11.1	15.4
R_{cen} (Å)[c]	3.69	3.77	3.65
$\beta_{HRS,800}$ (10^{-30} esu)	37 ± 4	74 ± 5	90 ± 5
$\beta_{HRS,\infty}$ (10^{-30} esu) TSA	14 ± 2	28 ± 2	38 ± 2
$\beta_{HRS,\infty}$ (10^{-30} esu) TSA (homog damping)	14 ± 2	29 ± 2	41 ± 2
$\beta_{HRS,\infty}$ (10^{-30} esu) TSA (homog + inhomog damping, vibr)	13 ± 2	25 ± 2	33 ± 2
$\beta_{HRS,\infty}$ (10^{-30} esu) CPHF, IEFPCM (water)	25	29	35
DR ($\lambda = \infty$) CPHF/IEFPCM (solvent = water)	4.20	4.42	5.92
$\beta_{HRS,1900}$ (10^{-30} esu) TDHF, IEFPCM (water)	12	16	19
$\beta_{HRS,1900}$ (10^{-30} esu) ONIOM+ (MP2:HF)	14	24	40

[a]pH-dependent.[46] [b]Measured at pH 7.5. [c]The centroids of all hydroxyphenyl rings of the chromophores and the phenyl ring of phenylalanine in eYFP Tyr203Phe are defined from their six carbon atoms. The centroid of the imidazole ring of His202 in zFP538 is defined from its five atoms. The atoms to define centroids and planes are identical. $\lambda_{abs,max}$: wavelength of maximal absorption; $\lambda_{em,max}$: wavelength of maximal emission; ε: extinction coefficient; τ: fluorescence lifetime; Φ: fluorescence quantum yield. Crystallographic average values for defining the relative orientation of the two aromatic rings in the chromophores: PDB ID: PDB identification code of the structure used; R_{cen}: centroid−centroid separation of the two rings of the chromophore having the $\pi-\pi$ stacking interactions; θ: center−normal angle of the hydroxyphenyl ring of the CR2 chromophore moiety; γ: normal−normal angle of the two planes of the hydroxyphenyl ring of the CR2 chromophore moiety and the aromatic side chain of the second chromophore moiety.[47] $\beta_{HRS,800}$: dynamic first hyperpolarizability; $\beta_{HRS,\infty}$: static first hyperpolarizability; TSA:[48] two-state approximation; DR: depolarization ratio; CPHF:[49] coupled-perturbed Hartree−Fock TDHF:[49] time-dependent Hartree−Fock; IEFPCM:[50] integral equation formalism polarizable continuum model; MP2:[39] second-order Møller−Plesset. ND: not determined.

cyclization of three amino acid residues, the chromophore of eYFP and SHardonnay contains a second moiety consisting of the aromatic side chains of Tyr203 and Phe203, respectively. The equivalent residue in zFP538 is His202, although the contribution of His202 to the chromophore and the optical properties was never fully investigated. The red shift of zFP538 can be accounted for by Lys66, creating a third ring with a CN double bond leading to an extension of the conjugated system, because the Lys66Met mutant of zFP538 restores green fluorescence.[52] His202 was therefore not suspected to play a vital role in the optical properties of the chromophore. Both conjugated moieties of the SHardonnay chromophore (the conjugated system originating from the Gly65-Tyr66-Gly67 triad, and Phe203, respectively) were modeled unambiguously in the electron density map (Figure 3). The two coplanar rings of the CR2 moiety adopt the cis conformation, and the two

dx.doi.org/10.1021/ja400098b | J. Am. Chem. Soc. 2013, 135, 4061−4069

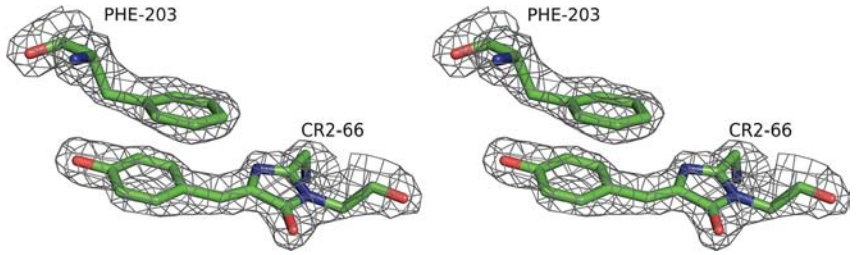

Figure 3. Stereoview of the SHardonnay chromophore, showing the final $2mF_o - DF_c$ map at 2.0σ level (gray mesh). The image was generated with PyMol.[45]

aromatic side chains align in an off-centered parallel displaced orientation.[47] Except for the minor modification, the deletion of the hydroxyl group in the hydroxyphenyl ring of Tyr203, the spatial arrangement of the chromophore atoms is conserved in SHardonnay (Figure 4 and Table 1).

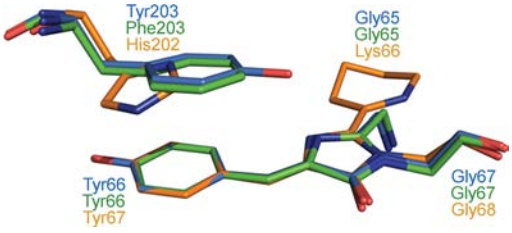

Figure 4. Superposition of the chromophores of SHardonnay (green) and zFP538 (orange) on eYFP (blue) after pair fitting of the atoms of the corresponding hydroxyphenyl moieties. The chromophores are displayed isolated from the protein barrel but including the (respectively) Tyr203, Phe203, and His202 residue close to the chromophore. The image was generated with PyMol.[45]

Experimental First Hyperpolarizability. We obtained the dynamic $\beta_{HRS,800}$ value from measurement with 800 nm femtosecond pulsed laser light and after correction for fluorescence contribution (Table 1).[53] The static hyperpolarizabilities, $\beta_{HRS,\infty}$, were then extrapolated from the measured $\beta_{HRS,800}$ by adopting different refinements of the two-state approximation (TSA) to evaluate the frequency dispersion factor (Table 1).[48]

Calculated First Hyperpolarizability. We obtained the calculated static and dynamic first hyperpolarizabilities by means of coupled-perturbed Hartree–Fock (CPHF) and time-dependent Hartree–Fock (TDHF) calculations,[49] Møller–Plesset second-order perturbation theory (MP2)[39] for deprotonated chromophores, and ONIOM+ calculations for the chromophores surrounded by the first shell of residues (Table 1). All levels of computation give the same amplitude ordering for β_{HRS}, i.e., β_{HRS} (eYFP) < β_{HRS} (SHardonnay) < β_{HRS} (zFP538), which also matches the experimental values, allowing therefore the use of these calculated data for the interpretation. An appropriate comparison in Table 1 should be based on the intrinsic or static β responses. Theoretically, the static responses were directly calculated at the MP2 level ($\beta_{HRS,\infty}$), while frequency-dependent $\beta_{HRS,1900}$ values, far from resonance, were also evaluated to account for a proper treatment of the solvent effects (with dynamic dielectric constant).

DISCUSSION

This report focuses on the effects of a minor modification in eYFP on its linear and nonlinear optical properties. On the basis of previous research,[5−8] we proposed to mutate the π-stacked Tyr203 into Phe203 to generate a yellow fluorescent protein with an improved β. This mutant, SHardonnay, shows linear spectral properties highly similar to those of eYFP, implying that stacking with Phe203 takes place and causes a comparable spectral shift. The blue shift of 2 nm points to a minimal reduction in the effective conjugation path length of the chromophore, due to elimination of the hydroxyl group of Tyr203. Even though the structural difference is almost negligible in terms of crystal structure and linear optical properties, it brings about a considerable increase in β for SHardonnay with respect to eYFP and restores the originally observed trend.[6−8] This confirms our earlier conjecture that the local centrosymmetry in the chromophore causes a substantial drop in the second-order optical performance of the fluorescent protein.

The molecular structure of the mutant was determined by X-ray diffraction, providing accurate coordinates of the atoms. Comparison of the chromophores at the molecular level confirmed the conservation of the aromatic ring in residue 203, except for a minimal translation of 0.08 Å. The knowledge of the chromophore structure and its nearby surroundings is also essential for accurate calculation of β by quantum chemical methods such as the ONIOM+ MP2:HF method applied to large systems (≈500 atoms) that was successfully used in this work.

Besides the Tyr203Phe mutant of eYFP, another, natural, fluorescent protein was investigated as an alternative approach for a yellow variant with an appreciable β value. The conjugated system in zFP538 is extended through the covalent bonds of the Lys66 residue[44,52] (Tyr68 being the chromophoric tyrosine equivalent) instead of the noncovalent π-stacking in most other known yellow fluorescent proteins. The conjugated path is slightly longer in zFP538 than in the yellow variants and coincides with a red shift in the linear spectrum and a larger β. This is in line with the general bandgap considerations of stronger nonlinearity (larger β) for a smaller bandgap (red-shifted absorption). The ONIOM+ MP2:HF method confirms the enhanced second-order nonlinear optical response in our mutant, though slightly overestimates that of zFP538. This may point to the very subtle interplay between conjugation extension and stacking to influence the bandgap for inducing a red shift, but this could also be due to imperfections in the crystal structure.

While SHardonnay was mainly designed to investigate our hypothesis and can be interpreted as a proof of principle, our ultimate goal is to engineer fluorescent proteins that can be used in SHG imaging. SHIM with eGFP as a voltage-sensitive contrast marker was demonstrated in *Caenorhabditis elegans*,[31] but no follow-up papers have been published so far. This suggests that fluorescent proteins as we know them, may not be

ideal markers for SHIM. We estimate that future work to optimize a number of parameters can result in successful SHG imaging with fluorescent proteins. These parameters include the size of the conjugated system of the chromophore, the choice of the fundamental wavelength, and the concentration, or density, of the chromophores as well as their relative orientation.

First of all, the strength of the second-harmonic response is related to the length of the effective conjugation path in the chromophore. The size of the planar chromophores of fluorescent proteins is limited by the eventual folding of the protein. With this report, we show that the conjugated system can also be extended noncovalently, without losing nonlinear optical performance.

Secondly, the use of longer wavelengths should be promoted for cellular SHIM. The contribution of resonance enhancement will then increase significantly, resulting in a realistic β_λ of 1 order of magnitude higher.[54] Good performance is expected for dyes with a β_λ around 300×10^{-30} esu,[24,55] but this could be an overestimation. Di-8-ANEPPS, together with di-4-ANEPPS a popular voltage sensitive marker in TPEF and SHG microscopy near 800 nm,[56,57] performs well with a β_{800} of about $200-350 \times 10^{-30}$ esu, depending on the medium (unpublished HRS results). While we measured a β_{800} of 134×10^{-30} esu for mCherry,[7] the estimated β_{1000} for mCherry, according to the TSA approximation, would be $290 \pm 60 \times 10^{-30}$ esu, which would make mCherry a good candidate for SHIM. Ideally, the design of SHG probes should aim for chromophores that allow to have all involved wavelengths within the optical window for biological tissue. The second-harmonic effect limits the options, but does not exclude optimization. Regardless of the choice of the wavelengths, the background signal from collagen, microtubules, or myosin should not be ignored, even in cultured live cells.[58]

A third point of concern in promoting fluorescent proteins versus small chemical dyes for SHG imaging is the maximal number of chromophores in the focus of the laser beam. A good working concentration for SHIM from membrane-associated dyes is estimated at 1 chromophore per 100 lipids.[55] This is harder to achieve with fluorescent proteins than with small chemical dyes because of their size, and for toxicity reasons. However, fluorescent proteins will reduce flip-flopping of the dye, reducing centrosymmetry, and internalization of the chromophore.

Last but not least, a very important issue in SHIM is the control of the relative orientation of the chromophores in the sample. There is a critical need to optimize this because the bulk second-order susceptibility ($\chi^{(2)}$), determining the final signal strength, depends on it. Cellular membranes are obviously convenient scaffolds to force chromophores in a parallel orientation, and as long as the molecules are not subject to flip-flopping or internalization, they could be arranged in a parallel and noncentrosymmetrical way. However, the use of membrane-targeted fluorescent proteins often involves a flexible linker of about 5 to 20 amino acids to ensure correct folding. This flexibility can be detrimental for the SHG signal, but possible solutions are available.[59−61]

CONCLUSIONS

On the basis of the findings of our previous research, we have altered eYFP by a single mutation to increase its surprisingly low first hyperpolarizability, β. Analysis by means of X-ray crystallography confirmed a correct folding with conservation of the relative position of the mutated Phe203 residue to the chromophore. The Tyr203Phe mutant of eYFP, dubbed SHardonnay, exhibits a minimal spectral shift, a similar fluorescence lifetime, and even an improved fluorescence quantum efficiency compared to the mother eYFP. Hyper-Rayleigh scattering measurements revealed a substantial increase in its β, hereby confirming our hypothesis as well as the disruption of the centrosymmetry in the chromophore.

We hereby confirm the importance of the noncentrosymmetry requirement for the second-order nonlinear optical properties and show the sensitivity of this principle. The removal of a hydroxyl group resulted in minor or no changes in the linear optical properties but a remarkable increase for the second-order properties. We therefore propose that the noncentrosymmetric stacking strategy could be explored in further research to extend the conjugated system in red fluorescent proteins, because a chromophoric tyrosine residue is present in the majority of fluorescent proteins. For substantial enhancement of the second-order optical properties, however, extension of the conjugated system through covalent interaction seems to be a stronger argument, but the size of the chromophore in fluorescent proteins is restricted by the microenvironment.

The importance of engineering fluorescent proteins with a high first hyperpolarizability becomes clear when considering the other difficulties in designing the experimental conditions that could result in images with SHG originating from the fluorescent proteins. Not only the strength of the individual molecular response, expressed by β, has to be maximized but also the molecular arrangement of the chromophores, their concentration, or density, will be important for the experiment. Also the choice of the fundamental wavelength is of vital importance, as it should be close enough to resonance conditions yet keep its distance from the fluorescence spectrum for successful SHIM based on fluorescent proteins. We speculate that our results offer a lot of potential to engineer new fluorescent proteins to explore new approaches for SHIM.

METHODS

Mutation and Plasmid Preparation. The zFP538 gene was amplified from the original pQE-30 UA plasmid using the primers gttcgctagcatggctcattcaaagcacggtctaaaag (forward) and gcacggatcctcaggccaaggcagaaggg (reverse) and cloned into the restriction sites *Nhe*I and *Bam*HI of a pET28a vector for expression. To generate the eYFP mutant, we mutated a pCRII-TOPO vector (Invitrogen kit) containing the eYFP gene in a PCR process using Pfu Ultra II and the primers caaccactacctgagctTccagtccgccctgagcaaagaccccaacg (forward) and ctcagggcggactggAagctcaggtagtggttgtcgggcagcagcacg (reverse). The capital letters refer to the mutation. The mutated eYFP gene was consequently cloned into the pET28a (Invitrogen) vector at the *Nhe*I and *Bam*HI sites.

Expression and Purification. The His_6-tagged proteins were expressed in *Escherichia coli* BL21 star (Invitrogen). Cells were lysed by incubation with lysozyme (hen egg white lysozyme, Invitrogen) followed by sonication and benzonase treatment (Sigma-Aldrich). The proteins were purified from the cell lysate by nickel affinity chromatography according to the manufacturer's instructions (HisTrap HP 5 mL column on an Äkta Purifier system, both GE Healthcare), followed by gel filtration chromatography on a Sephadex-200 column using a 20 mM 4-(2-hydroxyethyl)-1-piperazineethanesulfonic acid (HEPES) buffer with 250 mM NaCl. The protein was dialyzed against a 20 mM 2-(*N*-morpholino)ethanesulfonic acid (MES) buffer without NaCl for crystallography and concentrated using a Vivaspin 6 concentrator (Vivascience, cutoff 10 kDa). The

purity of the samples was assessed by means of SDS-PAGE and MALDI-TOF mass spectrometry (Bruker Ultraflex II).

Crystallization and Data Collection. Crystallization conditions of SHardonnay were screened using the 96-matrix Crystal Screen (Hampton Research) by the hanging drop vapor-diffusion method. Hanging drops consisted of 1 μL of SHardonnay (11 mg mL^{-1}) and 1 μL of the well solution and were placed against 500 μL of the screening solution in 24-well combo plates (Greiner Bio-One) at 289 K. Suitable crystals for X-ray diffraction were obtained after 2 days in 2 M ammonium sulfate and 0.1 M Tris-HCl (tris(hydroxymethyl)-aminomethane) pH 8.5. The crystals were swept through cryoprotectant (0.05 M Tris-HCl pH 8.5, 1 M $(NH_4)_2SO_4$, and 25% glycerol) and flash-frozen in liquid nitrogen prior to diffraction data collection.

Data collection and reduction: a 94% complete data set was collected on a MAR225 CCD detector with a wavelength of 1.00 Å, a φ range of 180°, an increment of 0.5°, and crystal-to-detector distance of 165 mm under a nitrogen cryostream of 100 K at the beamline PXIII of the Swiss Light Source (SLS) synchrotron in Villigen, Switzerland. Data were processed with XDS version December 6, 2010,[62] and scaled with SCALA 3.3.20[63] within the CCP4 suite.[64] Although the resolution edge of the diffraction pattern was 1.70 Å, after careful analysis, the data was truncated to 1.95 Å. The reflections on a single ice ring at 2.12 Å resolution had to be excluded during the integration. The crystal belonged to the tetragonal space group $P4_12_12$, with unit cell parameters $a = b = 59.86$, $c = 165.54$ Å. The data collection statistics are summarized in Table 2.

Table 2. Data Collection and Refinement Statistics

	SHardonnay (PDB ID 3V3D)
Data Collection	
space group	$P4_12_12$
cell dimensions	
a, *b*, *c* (Å)	59.86, 59.86, 165.54
resolution (Å)	56.29−1.95 (2.06−1.95)[a]
R_{merge}	0.045 (0.504)
$I/\sigma I$	30.4 (5.3)
completeness (%)	94.0 (99.2)
redundancy	13.9 (14.0)
Refinement	
resolution (Å)	56.29−1.95
no. reflections	21520
R_{work}/ R_{free}	0.1868/0.2293
no. atoms	
protein	1823
ligand/ion	5
water	229
B-factors (Å^2)	
protein	44.9
ligand/ion	81.7
water	55.3
rms deviations	
bond lengths (Å)	0.009
bond angles (deg)	1.323

[a]Values for the highest resolution shell are shown in parentheses.

Phasing and Refinement. The SHardonnay structure was solved by molecular replacement, using the program Phaser 2.1.4,[65] integrated in the CCP4 suite. The coordinates of the A chain of YFP (PDB ID 1F0B)[66] were used as search model, with the chromophore omitted. Both the chromophore and the mutated residue were consequently modeled into the unambiguous electron density map with the program Coot 0.6.1[67] after subsequent cycles of refinement. Refinement was performed by *phenix.refine* GUI[68] using the standard dictionary files for amino acid residues and for a sulfate ion. Target values for the CR2 chromophore moiety were derived from crystal structures in the Cambridge Structural Database.[69]

The likelihood-based refinement converged to R_{work} and R_{free} values of 0.1845 and 0.2293, respectively, for in total 2057 atoms and 21 520 unique reflections (Table 2). The structure was refined with 232 (from 2 to 233) of in total 238 amino acid residues defined. Most of the residues are well fitted in the electron density, except for the paucity of electron density in the side chains of amino acid residues Lys3, Glu6, Lys52, Glu90, Glu132, Lys156, Lys162, and Lys214. They are either located in loops or exposed to the solvent, indicating disorder; therefore, coordinates of these atoms were removed as being unreliable. A sulfate ion could be reasonably modeled in the electron density observed near Arg73. A total of 229 water molecules were included in the model using the "water update" option integrated in *phenix.refine* GUI; if they were within hydrogen bonding distance to chemically reasonable groups, they appeared in $mF_o - DF_c$ maps contoured at 3.0σ and had a *B*-factor less than 80 Å^2. None of the residues are found in disallowed regions, and 98.7% of the residues are in the favored region of the Ramachandran plot (calculated with MolProbity: http://molprobity.biochem.duke.edu/). The atomic coordinates and structure factors of SHardonnay have been deposited in the Protein Data Bank[70] (www.pdb.org; accession code 3V3D).

Optical Characterization. The fluorescence spectra and all spectra necessary for the determination of the fluorescence quantum yield were measured on a Synergy MX monochromator-based multimode microplate reader (Biotek). The achieved fluorescence quantum yield of SHardonnay was successfully cross-checked with that of purified eGFP and eYFP. For the determination of the protein concentrations necessary to derive an extinction coefficient, the Bradford method was used. All required absorption values (A_{595} of Bradford solutions, A_{280} of Bovine Serum Albumin, A_{280} and A_{511} of SHardonnay as well as the linear absorption spectra) were measured in 1 cm quartz cuvettes in a Genesys 6 spectrophotometer (ThermoScientific).

The first hyperpolarizability, β, was experimentally determined by frequency-resolved femtosecond hyper-Rayleigh scattering (HRS), as described previously.[6] To estimate the intrinsic β response, the experimental data were pretreated to eliminate resonance effects.[71,72] The frequency dispersion factors, $F(\omega,\omega_{ge},\gamma) = \beta_{zzz}(-2\omega;\omega,\omega)/\beta_{zzz}(0;0,0)$, were determined from successive refinements of the two-state approximation (TSA),[48] a good approximation for pseudodipolar chromophores with one excited state dominating the second-order nonlinear optical response. Besides the conventional TSA, homogeneous damping was employed within the TSA. Further improvements on the static β quantities were made by incorporating an inhomogeneous broadening based on the absorption spectrum, which implicitly contains information on the distribution of the transition frequencies as well as by taking into account the vibronic structure of the excited states.[71,72] To apply these extrapolation schemes, the successive $F(\omega,\omega_{ge},\gamma)$ functions had to be fitted to the UV/vis absorption spectra using the parameters in Table S1, Supporting Information. The corresponding simulated absorption spectra are compared with the experimental spectra (Figure 2), demonstrating a very close relationship between the two.

Computational Methods and Geometrical Structures. The geometries of all chromophores and surrounding residues were extracted from available X-ray diffraction data.[40,52] The position of the H atoms at the density functional theory (DFT) level using the B3LYP exchange-correlation functional and the 6-31+G* basis set for the chromophores (Figure S1, Supporting Information) but with the PM6 method for the chromophores surrounded by the first shell of residues.

The first hyperpolarizabilities (β) determined by the second-order Møller−Plesset (MP2) method recover the largest part of the electron correlation effects.[39] First, the static β values were calculated using the finite field (FF) procedure implying a Romberg scheme to improve the accuracy on the numerical derivative.[73] Then the multiplicative scheme[74] was used to account for frequency dispersion (λ = 1900 nm):

$$\beta_{MP2}(-2\omega;\omega,\omega) \approx \beta_{MP2}(0;0,0) \times \frac{\beta_{TDHF}(-2\omega;\omega,\omega)}{\beta_{CPHF}(0;0,0)}$$

where the frequency-dependence is described at the Hartree−Fock (HF) level by combining the time-dependent Hartree−Fock (TDHF) and the coupled-perturbed Hartree−Fock (CPHF) schemes for obtaining the dynamic (or frequency-dependent) and the static values, respectively.[49] The static values extrapolated from experiment are best compared with the calculated low-frequency dynamic values to account for the optical dielectric constant of the environment.

The chromophore environment was modeled by employing (i) the polarizable continuum model within the integral equation formalism polarizable continuum model (IEFPCM)[50] in CPHF/TDHF calculations and (ii) the ONIOM approach,[75] which explicitly takes the first shell of residues into account. The outer layer is described at the HF level whereas the MP2 scheme is adopted for the inner region consisting of the chromophore. The 6-31+G* basis set was adopted because valence polarization double-ζ + polarization basis sets with one set of diffuse functions are suitable to reproduce within about 5% the β values of push−pull π conjugated molecules calculated with much extended basis sets.[39] Taking advantage of using the same basis set for the two layers, there is a nice cancelation of terms in the ONIOM energy expression

$$E_{ONIOM+} = E_{real,HF} + E_{model,E2}$$

and similarly for β. The only remaining approximation comes from the use of the MP2 scheme to describe the correlation energy, which is evaluated on the model system. This ONIOM scheme, applied to correlation effects only, was named the ONIOM+ method.

The reported quantities are related to the HRS experiments with plane-polarized incident laser light and the observation made perpendicular to the propagation plane. Then, the full intensity reads

$$\beta_{HRS}(-2\omega;\omega,\omega) = \sqrt{\langle\beta_{ZZZ}^2\rangle + \langle\beta_{ZXX}^2\rangle}$$

whereas the depolarization ratio (DR) is given by

$$DR = \frac{\langle\beta_{ZZZ}^2\rangle}{\langle\beta_{ZXX}^2\rangle}$$

The $\langle\beta_{ZZZ}^2\rangle$ and $\langle\beta_{ZXX}^2\rangle$ terms correspond to orientational averages of all the β tensor components in the molecular frame. The DR gives information on the geometry of the part of the molecule responsible for the nonlinear optical (NLO) response, also called the NLO-phore. All reported β values are given in 10^{-30} esu (10^{-30} esu = 115.7 au) within the B convention. All calculations were performed with mopac2009[76], Gaussian09[77] as well as homemade codes.

■ ASSOCIATED CONTENT

Supporting Information

Figure S1: Models of the isolated chromophores used for the Gaussian calculations. (a) the eYFP chromophore model, (b) SHardonnay and (c) zFP538. Table S1: Best parameters fitting the UV/vis absorption spectra. Atomic coordinates of chromophores used for the CPHF/TDHF calculations (coord_SHardonnay-small.xyz; coord_eYFP-small.xyz, and coord_zFP538-small.xyz files). Atomic coordinates of chromophores surrounded by the first shell of residues used for the ONIOM+ calculations (coord_eYFP-big.xyz; coord_SHardonnay-big.xyz and coord_zFP538-big.xyz files). The CIF file of SHardonnay (SHardonnay.mmcif). This material is available free of charge via the Internet at http://pubs.acs.org.

■ AUTHOR INFORMATION

Corresponding Author

koen.clays@fys.kuleuven.be.

Present Address

[#]Department of Inorganic and Physical Chemistry, Ghent University, Krijgslaan 281 - S3, BE-9000 Ghent, Belgium.

Notes

The authors declare no competing financial interest.

■ ACKNOWLEDGMENTS

The original pQE-30 UA plasmid containing the zFP538 gene was obtained from J.S. Remington (University of Oregon), and the authors thank him for this generous gift. The authors also thank M. Deng and Y. Engelborghs (KU Leuven) for the fluorescence lifetime measurements. E.D.M. and K.C. thank the Institute for Nanoscale Physics and Chemistry (INPAC), the Flemish Research Fund (FWO, grant no. G.0484.12) and the KU Leuven Research Fund for financial support. N.N.B. is funded by a Ph.D. grant from the Vietnamese government (project 322) and KU Leuven. N.N.B., K.V.H., and L.V.M. thank the staff at the Swiss Light Source (beamline PXIII) at the Paul Scherrer Institute in Villigen, Switzerland, for access and technical assistance with the synchrotron experiments. The calculations have been performed at the Interuniversity Scientific Computing Facility (iSCF), installed at the FUNDP, for which M.deW. and B.C. gratefully acknowledge the financial support of the F.R.S.-FRFC under conventions No. 2.4.617.07.F and of the FUNDP.

■ REFERENCES

(1) Vanzi, F.; Sacconi, L.; Cicchi, R.; Pavone, F. S. *J. Biomed. Opt.* **2012**, *17*, 060901.
(2) Campagnola, P. J. *Anal. Chem.* **2011**, *83*, 3224−3231.
(3) Min, W.; Freudiger, C. W.; Lu, S.; Xie, X. S. *Annu. Rev. Phys. Chem.* **2011**, *62*, 507−530.
(4) Brown, E.; McKee, T.; diTomaso, E.; Pluen, A.; Seed, B.; Boucher, Y.; Jain, R. K. *Nat. Med.* **2003**, *9*, 796−800.
(5) Asselberghs, I.; Flors, C.; Ferrighi, L.; Botek, E.; Champagne, B.; Mizuno, H.; Ando, R.; Miyawaki, A.; Hofkens, J.; Van der Auweraer, M.; Clays, K. *J. Am. Chem. Soc.* **2008**, *130*, 15713.
(6) De Meulenaere, E.; Asselberghs, I.; de Wergifosse, M.; Botek, E.; Spaepen, S.; Champagne, B.; Vanderleyden, J.; Clays, K. *J. Mater. Chem.* **2009**, *19*, 7514−7519.
(7) De Meulenaere, E.; Vanderlinden, W.; Vanderleyden, J.; Clays, K. *Proc. SPIE* **2010**, *7765*, 77650−77658.
(8) De Meulenaere, E.; de Wergifosse, M.; Botek, E.; Spaepen, S.; Champagne, B.; Vanderleyden, J.; Clays, K. *J. Nonlinear Opt. Phys.* **2010**, *19*, 1−13.
(9) Sheppard, C. J. R.; Gu, M. *Optik* **1990**, *86*, 104−406.
(10) Denk, W.; Strickler, J. H.; Webb, W. W. *Science* **1990**, *248*, 73−76.
(11) So, P. T. C.; Dong, C. Y.; Masters, B. M.; Berland, K. M. *Annu. Rev. Biomed. Eng.* **2000**, *2*, 399−429.
(12) Helmchen, F.; Denk, W. *Nat. Methods* **2005**, *2*, 932−940.
(13) Nucciotti, V.; Stringari, C.; Sacconi, L.; Vanzi, F.; Fusi, L.; Linari, M.; Piazzesi, G.; Lombardi, V.; Pavone, F. S. *Proc. Natl. Acad. Sci. U.S.A.* **2010**, *107*, 7763−7768.
(14) Campagnola, P. J.; Loew, L. M. *Nat. Biotechnol.* **2003**, *21*, 1356−1360.
(15) Bianchini, P.; Diaspro, A. *J. Biophoton.* **2008**, *1*, 443−50.
(16) Campagnola, P. J.; Millard, A. C.; Terasaki, M.; Hoppe, P. E.; Malone, C. J.; Mohler, W. A. *Biophys. J,.* **2002**, *82*, 493−508.
(17) Cicchi, R.; Kapsokalyvas, D.; De Giorgi, V.; Maio, V.; Van Wiechen, A.; Massi, D.; Lotti, T.; Pavone, F. S. *J. Biophoton.* **2010**, *3*, 34−43.
(18) Mohler, W.; Millard, A. C.; Campagnola, P. J. *Methods* **2003**, *29*, 97−109.
(19) Salafsky, J. S.; Cohen, B. A *J. Phys. Chem. B* **2008**, *112*, 15103−15107.

(20) Plotnikov, S. V.; Millard, A. C.; Campagnola, P. J.; Mohler, W. A. *Biophys. J.* **2006**, *90*, 693−703.
(21) Tiaho, F.; Recher, G.; Rouede, D. *Opt. Express* **2007**, *15*, 12286−12295.
(22) Psilodimitrakopoulos, S.; Amat-Roldan, I.; Loza-Alvarez, P.; Artigas, D. *J. Opt.* **2010**, *12*, 084007.
(23) Duboisset, J.; Aït-Belkacem, D.; Roche, M.; Rigneault, H.; Brasselet, S. *Phys. Rev. A* **2012**, *85*, 043829.
(24) De Meulenaere, E.; Chen, W.-Q.; Van Cleuvenbergen, S.; Zheng, M.-L.; Psilodimitrakopoulos, S.; Paesen, R.; Taymans, J.-M.; Ameloot, M.; Vanderleyden, J.; Loza-Alvarez, P.; Duan, X.-M.; Clays, K. *Chem. Sci.* **2012**, *3*, 984−995.
(25) Dombeck, D. A.; Sacconi, L.; Blanchard-Desce, M.; Webb, W. W. *J. Neurophysiol.* **2005**, *94*, 3628−3636.
(26) Barsu, S.; Cheaib, R.; Chambert, S.; Queneau, Y.; Maury, O.; Cottet, D.; Wege, H.; Douady, J.; Bretonnière, Y.; Andraud, C. *Org. Biomol. Chem.* **2010**, *8*, 142−150.
(27) Theer, P.; Denk, W.; Sheves, M.; Lewis, A.; Detwiler, P. B. *Biophys. J.* **2011**, *100*, 232−242.
(28) Millard, A. C.; Jin, L.; Wei, M. D.; Wuskell, J. P.; Lewis, A.; Loew, L. M. *Biophys. J.* **2004**, *86*, 1169−1176.
(29) Reeve, J. E.; Collins, H. A.; De Mey, K.; Kohl, M. M.; Thorley, K. J.; Paulsen, O.; Clays, K.; Anderson, H. L. *J. Am. Chem. Soc.* **2009**, *131*, 2758−2759.
(30) Liao, Y.; Eichinger, B. E.; Firestone, K. A.; Haller, M.; Luo, J.; Kaminsky, W.; Benedict, J. B.; Reid, P. J.; Jen, A.K-Y.; Dalton, L.; Robinson, B. H. *J. Am. Chem. Soc.* **2005**, *127*, 2758−2766.
(31) Khatchatouriants, A.; Lewis, A.; Rothman, Z.; Loew, L.; Treinin, M. *Biophys. J.* **2000**, *79*, 2345−2352.
(32) Shaner, N. C.; Lin, M. Z.; McKeown, M. R.; Steinbach, P. A.; Hazelwood, K. L.; Davidson, M. W.; Tsien, R. Y. *Nat. Methods* **2008**, *5*, 545−551.
(33) Shaner, N. C.; Steinbach, P. A.; Tsien, R. Y. *Nat. Methods* **2005**, *2*, 905−909.
(34) Subach, F. V.; Piatkevich, K. D.; Verkhusha, V. V. *Nat. Methods* **2011**, *8*, 1019−1026.
(35) Piljić, A.; de Diego, I.; Wilmanns, M.; Schultz, C. *ACS Chem. Biol.* **2011**, *6*, 685−691.
(36) Truong, K.; Sawano, A.; Mizuno, H.; Hama, H.; Tong, K. I.; Mal, T. K.; Miyawaki, A.; Ikura, M. *Nat. Struct. Biol.* **2001**, *8*, 1069−1073.
(37) Betzig, E.; Patterson, G. H.; Sougrat, R.; Lindwasser, O. W.; Olenych, S.; Bonifacino, J. S.; Davidson, M. W.; Lippincott-Schwartz, J.; Hess, H. F. *Science* **2006**, *313*, 1642−1645.
(38) Xiong, A.; Peng, R. H.; Zhuang, J.; Davies, J.; Zhang, J.; Yao, Q. H. *Crit. Rev. Biotechnol.* **2012**, *32*, 133−142.
(39) de Wergifosse, M.; Champagne, B. *J. Chem. Phys.* **2011**, *134*, 074113.
(40) Wachter, R. M.; Elsliger, M. A.; Kallio, K.; Hanson, G. T.; Remington, S. J. *Structure* **1998**, *6*, 1267−1277.
(41) Rekas, A.; Alattia, J. R.; Nagai, T.; Miyawaki, A.; Ikura, M. *J. Biol. Chem.* **2002**, *277*, 50573−50578.
(42) Clays, K.; Hendrickx, E.; Triest, M.; Verbiest, T.; Persoons, A.; Dehu, C.; Brédas, J.-L. *Science* **1993**, *262*, 1419−1421.
(43) Matz, M. V.; Fradkov, A. F.; Labas, Y. A.; Savitsky, A. P.; Zaraisky, A. G.; Markelov, M. L.; Lukyanov, S. A. *Nat. Biotechnol.* **1999**, *17*, 969−973.
(44) Pletneva, N. V.; Pletnev, S. V.; Chudakov, D. M.; Tikhonova, T. V.; Popov, V. O.; Martynov, V. I.; Wlodawer, A.; Dauter, Z.; Pletnev, V. Z. *Russ. J. Bioorgan. Chem.* **2007**, *33*, 390−398.
(45) DeLano, W. L. *Pymol*, DeLano Scientific LLC, Palo Alto, CA, 2008.
(46) Borst, J. W.; Hink, M. A.; van Hoek, A.; Visser, A. J. W. G. *J. Fluoresc.* **2005**, *15*, 153−160.
(47) McGaughey, G. B.; Gagné, M.; Rappé, A. K. *J. Biol. Chem.* **1998**, *273*, 15458−15463.
(48) Oudar, J. L.; Chemla, D.S. . *J. Chem. Phys.* **1977**, *66*, 2664−2668.
(49) Karna, S. P.; Dupuis, M. *J. Comput. Chem.* **1991**, *12*, 487−504.
(50) Tomasi, J.; Mennucci, B.; Cammi, R. *Chem. Rev.* **2005**, *105*, 2999−3093.
(51) Krissinel, E.; Henrick, K. *Acta Crystallogr., Sect. D: Biol. Crystallogr.* **2004**, *60*, 2256−2268.
(52) Remington, S. J.; Wachter, R. M.; Yarbrough, D. K.; Branchaud, B.; Anderson, D. C.; Kallio, K.; Lukyanov, K. A. *Biochemistry* **2005**, *44*, 202−212.
(53) Olbrechts, G.; Strobbe, R.; Clays, K.; Persoons, A. *Rev. Sci. Instrum.* **1998**, *69*, 2233−2241.
(54) De Mey, K.; Perez-Moreno, J.; Reeve, J. E.; Lopez-Duarte, I.; Boczarow, I.; Anderson, H. L.; Clays, K. *J. Phys. Chem. C* **2012**, *116*, 13781−13787.
(55) Reeve, J. E.; Anderson, H. L.; Clays, K. *Phys. Chem. Chem. Phys.* **2010**, *12*, 13484−14498.
(56) Reeve, J. E.; Corbett, A. D.; Boczarow, I.; Wilson, T.; Bayley, H.; Anderson, H. L. *Biophys. J.* **2012**, *103*, 907−917.
(57) Millard, A. C.; Terasaki, M.; Loew, L. M. *Biophys. J.* **2005**, *88*, L46−L48.
(58) De Meulenaere, E.; Paesen, R.; Psilodimitrakopoulos, S.; Ameloot, M.; P. Loza-Alvarez, P.; Vanderleyden, J.; Clays, K. *Proc. SPIE* **2012**, *8226*, 82263C.
(59) Lazar, J.; Bondar, A.; Timr, S.; Firestein, S. J. *Nat. Methods* **2011**, *8*, 684−690.
(60) Knopfel, T.; Tomita, K.; Shimazaki, R.; Sakai, R. *Methods* **2003**, *30*, 42−48.
(61) Kress, A.; Ferrand, P.; Rigneault, H.; Trombik, T.; He, H.-T.; Marguet, D.; Brasselet, S. *Biophys. J.* **2011**, *101*, 468−476.
(62) Kabsch, W. *Acta Crystallogr., Sect. D: Biol. Crystallogr.* **2010**, *66*, 125−132.
(63) Evans, P. R. *Acta Crystallogr., Sect. D: Biol. Crystallogr.* **2006**, *62*, 72−82.
(64) Collaborative Computational Project, Number 4. *Acta Crystallogr., Sect. D: Biol. Crystallogr.* **1994**, *50*, 760−763.
(65) McCoy, A. J.; Grosse-Kunstleve, R. W.; Adams, P. D.; Winn, M. D.; Storoni, L. C.; Read, R. J. *J. Appl. Crystallogr.* **2007**, *40*, 658−674.
(66) Wachter, R. M.; Yarbrough, D.; Kallio, K.; Remington, S. J. *J. Mol. Biol.* **2000**, *301*, 157−171.
(67) Emsley, P.; Lohkamp, B.; Scott, W. G.; Cowtan, K. *Acta Crystallogr., Sect. D: Biol. Crystallogr.* **2010**, *66*, 486−501.
(68) Adams, P. D.; Afonine, P. V.; Bunkoczi, G.; Chen, V. B.; Davis, I. W.; Echols, N.; Headd, J. J.; Hung, L. W.; Kapral, G. J.; Grosse-Kunstleve, R. W.; McCoy, A. J.; Moriarty, N. W.; Oeffner, R.; Read, R. J.; Richardson, D. C.; Richardson, J. S.; Terwilliger, T. C.; Zwart, P. H. *Acta Crystallogr., Sect. D: Biol. Crystallogr.* **2010**, *66*, 213−221.
(69) Allen, F. H. *Acta Cryst. B* **2002**, *58*, 380−388.
(70) Berman, H. M.; Westbrook, J.; Feng, Z.; Gilliland, G.; Bhat, T. N.; Weissig, H.; Shindyalov, I. N.; Bourne, P. E. *Nucleic Acids Res.* **2000**, *28*, 235−242.
(71) Campo, J.; Wenseleers, W.; Goovaerts, E.; Szablewski, M.; Cross, G. H. *J. Phys. Chem. C* **2008**, *112*, 287−296.
(72) Mançois, F.; Pozzo, J. L.; Pan, J. F.; Adamietz, F.; Rodriguez, V.; Ducasse, L.; Castet, F.; Plaquet, A.; Champagne, B. *Chem.—Eur. J.* **2009**, *15*, 2560−2571.
(73) Cohen, H. D.; Roothaan, C. C. J. *J. Chem. Phys.* **1965**, *43*, S34.
(74) Sekino, H.; Bartlett, R. J. *J. Chem. Phys.* **1986**, *85*, 976−989.
(75) Dapprich, S.; Komaromi, I.; Byun, K. S.; Morokuma, K.; Frisch, M. J. *J. Mol. Struct. (THEOCHEM)* **1999**, *461*−*462*, 1−21.
(76) Stewart, J. J. P. *MOPAC2009*, Stewart Computational Chemistry, Colorado Springs, CO.
(77) Frisch, M. J.; Trucks, G. W.; Schlegel, H. B.; Scuseria, G. E.; Robb, M. A.; Cheeseman, J. R.; Scalmani, G.; Barone, V.; Mennucci, B.; Petersson, G. A.; Nakatsuji, H.; Caricato, M.; Li, X.; Hratchian, H. P.; Izmaylov, A. F.; Bloino, J.; Zheng, G.; Sonnenberg, J. L.; Hada, M.; Ehara, M.; Toyota, K.; Fukuda, R.; Hasegawa, J.; Ishida, M.; Nakajima, T.; Honda, Y.; Kitao, O.; Nakai, H.; Vreven, T.; Montgomery, J. A., Jr.; Peralta, J. E.; Ogliaro, F.; Bearpark, M.; Heyd, J. J.; Brothers, E.; Kudin, K. N.; Staroverov, V. N.; Kobayashi, R.; Normand, J.; Raghavachari, K.; Rendell, A.; Burant, J. C.; Iyengar, S. S.; Tomasi, J.; Cossi, M.; Rega, N.; Millam, J. M.; Klene, M.; Knox, J. E.; Cross, J. B.; Bakken, V.;

Adamo, C.; Jaramillo, J.; Gomperts, R.; Stratmann, R. E.; Yazyev, O.; Austin, A. J.; Cammi, R.; Pomelli, C.; Ochterski, J. W.; Martin, R. L.; Morokuma, K.; Zakrzewski, V. G.; Voth, G. A.; Salvador, P.; Dannenberg, J. J.; Dapprich, S.; Daniels, A. D.; Farkas, Ö.; Foresman, J. B.; Ortiz, J. V.; Cioslowski, J.; Fox, D. J. *Gaussian 09, Revision C.02*, Gaussian, Inc., Wallingford, CT, 2010.